UV Photodissociation Dynamics of HN_3 in 190-248 nm

2007 Chin. J. Chem. Phys. 20 345

(http://iopscience.iop.org/1003-7713/20/4/04)

ARTICLE

UV Photodissociation Dynamics of HN_3 in 190-248 nm†

Jian-yang Zhang[a,c], Kai-jun Yuan[a], Yuan Cheng[a], Steven A. Harich[a], Xiu-yan Wang[a,c], Xue-ming Yang[a*], Alec M. Wodtke[b]

a. Dalian Institute of Chemical Physics, Chinese Academy of Sciences, Dalian 116023, China;
b. Department of Chemistry and Biochemistry, University of California at Santa Barbara, Santa Barbara 93106, USA;
c. Department of Physics, Dalian University of Technology, Dalian 116023, China

(Dated: Received on July 9, 2007; Accepted on August 2, 2007)

The H+N_3 channel in the ultraviolet photodissociation of HN_3 has been investigated from 190 nm to 248 nm using the high-n Rydberg H-atom time-of-flight technique. Product translational energy distributions as well as product angular anisotropy parameters were determined for the H+N_3 channel at different photolysis wavelengths. N_3 vibrational state distribution has also been derived from the product translational energy distribution at these wavelengths. Above photolysis wavelength 225 nm, HN_3 predominantly dissociate through the repulsive state. Below 225 nm, a new slow channel starts to appear at 220 nm in addition to the existing channel. This channel is attributed to a ring closure dissociation channel to produce the cyclic N_3 product. As photolysis energy increases, this new channel becomes more important.

Key words: Photodissociation dynamics, H atom channel, UV photolysis, Product vibrational state distribution

I. INTRODUCTION

The absorption spectrum of HN_3 is composed of at least three absorption systems between 180-300 nm: a weak one peaking at 264.3 nm and two strong ones peaking at 204 and 190 nm, respectively [1-4]. These absorption features are broad and nearly structureless. The weak feature at λ>220 nm has been assigned to $A\mathrm{A}''\leftarrow X\mathrm{A}'$ [2,3,5]. At shorter wavelengths, the $B\mathrm{A}'$ and $C\mathrm{A}''$ electronic states are optically accessible, and the resulting UV absorption spectrum is strong, but no discrete structure is present.

It is known that the UV photodissociation of HN_3 occurs primarily via two spin-allowed channels [1-16]:

$$\mathrm{HN_3}(X\mathrm{A}') \rightarrow \mathrm{H}(^2\mathrm{S}) + \mathrm{N_3}(X^2\Pi_\mathrm{g}) \quad (1)$$

$$\rightarrow \mathrm{NH}(a^1\Delta) + \mathrm{N_2}(X^1\Sigma_\mathrm{g}^+) \quad (2)$$

The NH+N_2 channel has been extensively studied at several different wavelengths [4,6-11]. NH is produced in the lowest singlet ($a^1\Delta$) instead of the $X^3\Sigma^-$ ground state because of the spin symmetry rule. The H-atom has been investigated by Comes and coworkers by laser induced fluorescence method [12,13], and H-ion TOF spectra [14]. The average center-of-mass translation energy ($\langle E_{\mathrm{trans}}\rangle$) release has been found to be 68% of the total available energy at 248 nm. The H atom quantum yield has been measured at several wavelengths: ϕ_{266}=0.04, ϕ_{248}=0.20. At 266 and 248 nm, the product anisotropy parameter is close to −1, indicating a perpendicular electronic transition ($A\mathrm{A}''\leftarrow X\mathrm{A}'$). Using the H-ion TOF spectra method [14], H−N bond energy is determined to be: D_0(H−N_3)=30850±400 cm^{-1}. The main structures observed in the distribution were assigned to a progression in the v_1 symmetric stretching mode of N_3 and the relative population of the (0,0,0):(1,0,0):(2,0,0):(3,0,0):(4,0,0) modes was found to be 0.09:0.19:0.28:0.29:0.15. Contributions to the TOF profile from other active vibrations could not be ruled out, because the resulting H^+ TOF profile was poorly resolved.

Recently, the high-n Rydberg H-atom time-of-flight (TOF) technique has also been employed to investigate the H-atom channel. Cook *et al.* reported the translational energy spectra of the H+$N_3(X)$ products following excitation at eight different excitation wavelengths ($\lambda \geq$240 nm) [15]. Based on their experimental results and analysis, they concluded that the N_3 fragments are formed in a progression of levels involving both the symmetric stretch mode (v_1,0,0) and the symmetric stretch mode combined with one and two quanta of bending motion, v_2. The rotational energy disposal in the $N_3(X)$ products was also estimated using an impulsive dissociation model, suggesting that the most probable impact parameter b is 1.26±0.05 Å. The dissociation energy of the H−N_3 bond is determined to be, D_0(H−N_3)=30970±50 cm^{-1}. The $N_3(X)$ vibrational state population distributions are determined at eight photolysis wavelengths. Zhang *et al.* have also used Rydberg H atom TOF method to investigate the HN_3 photodissociation at 248.3 and 193.3 nm [16]. At 248.3 nm, Zhang *et al.* assigned the vibrational structures in the product translational energy spectra, similar to Ref.[15]. The H−N_3 bond energy was determined to be D_0(H−N_3)=31020±180 cm^{-1}. At 193.3 nm, they

†Part of the special issue "Cun-hao Zhang Festschrift".
*Author to whom correspondence should be addressed. E-mail: xmyang@dicp.ac.cn

found that the product anisotropy parameter is clearly energy-dependent, implying multiple dissociation pathways are responsible.

The spectroscopy of N_3 is rather complicated due to several interactions (Renner-Teller and spin-orbit splitting, etc.) [17-20]. Early studies demonstrated an absorption band which was attributed to an electronic transition at ∼270 nm [17]. The ground state exhibits a spin-orbit splitting of $A_{0,\text{eff}}$=−71.26 cm^{-1}, and a Renner-Teller splitting of $\varepsilon\omega_2$=−94.38 cm^{-1} for the bending vibration. Subsequent wavelength dispersed LIF studies [18] yielded approximate values for the ground state symmetric stretch and bending vibrational frequencies of ω_1=1320 cm^{-1} and ω_2=457 cm^{-1} respectively. The asymmetric stretch frequency (ω_3=1644.678 cm^{-1} [19]) has been studied by Fourier transform spectroscopy, and laser magnetic resonance [20]. Recent calculation [21] reported a linear symmetric ground state with two equal N−N bond lengths of 1.1818 Å in good agreement with the experimental value [19,20]. Meier *et al.*'s calculation showed that the $HN_3(A)$ state PES indicates a barrier (with an estimated barrier height ∼2300 cm^{-1}) along the H−N_3 dissociation coordinate.

In this work, we re-investigated the photodissociation dynamics of the HN_3 molecule at different wavelengths lower than 248 nm in an effort to study how the dynamics changes when the photolysis energy increases.

II. EXPERIMENTS

The technique of H/D Rydberg atom TOF spectra technique has been described in detail elsewhere [22-24]. In this experiment, a skimmed, pulsed molecular beam of HN_3, seeded in helium (mixing ratio ∼2%, total pressure ∼101 kPa), is crossed perpendicularly with the photolysis laser beam. In the wavelength range of 225-280 nm, a frequency doubled dye laser (Sirah, PESC-G-24) pumped by a Nd:YAG (Spectra Physics Pro-290) is used. Laser wavelengths in the range of 188 nm to 225 nm are generated by frequency mixing of the second harmonic of the dye laser output with the Nd:YAG fundamental (1064 nm), using a second BBO crystal. The H-atom products from the photodissociation were excited to a high-n Rydberg level using a two-step excitation scheme: 121.6 nm excitation to the n=2 level from the ground state and the subsequent 366 nm excitation to a high-n (n∼45) Rydberg level from the n=2 state. The 121.6 nm light was generated by four-wave mixing of two 212.5 nm photons and one 845 nm photon in a Kr/Ar mixing cell. The 212.5 nm light was generated by doubling the output of a dye laser (Sirah, PESC-G-24) operating at ∼425 nm, which was pumped by a second Nd:YAG laser (Spectra Physics Pro-290) operating at 355 nm. The 845 nm light was the direct output of a dye laser (Continue ND6000) pumped by the 532 nm output of the same Nd:YAG laser. These laser beams were then focused into a cell with Kr/Ar mixing gas where four wave mixing at 121.6 nm was generated. The 366 nm light was generated by frequency doubling a Radiant dye laser output (Jaguar, D90MA), operating at ∼732 nm, which was pumped by a port of the 532 nm light of the same Nd:YAG laser to excite the H atoms from the n=2 level to a high-n Rydberg state below the ionization threshold. The two 121.6 and 366 nm laser beams were overlapped exactly in the interaction region both in space and in time. Ions and electrons formed in this region were extracted by a small electric field placed across the interaction region.

The tagged H atoms then fly away from the interaction region to reach the MCP detector. The Rydberg H atoms are efficiently ionized as soon as they pass a fine grounded metal grid in front of the MCP detector by the strong electric field applied to the front MCP plate. The total distance from the interaction region to the front face of the detector is ∼333 mm. The signal obtained is amplified by a preamplifier, discriminated by a discriminator, sent to both a digital oscilloscope for visual display and a multi-channel scaler (P7888-2(E) FASTCOMTEC) for accumulation (typically more than 10^5 laser shots per TOF profile) and subsequent data analysis.

HN_3 was prepared by heating sodium azide (NaN_3) in excess stearic acid under vacuum for 3-4 h at 80-100 °C [24,25]. The HN_3 sample was stored in a stainless steel container and He gas was filled to produce 2% HN_3/He ratio (the total pressure made up to 101-404 kPa with pure helium). Purity was checked by mass spectrometry (SRS, RGA200).

III. RESULTS AND DISCUSSION

A. Dissociation dynamics from 230 nm to 264 nm

The time-of-flight spectra (TOF) of the H-atom product from the photodissociation of HN_3 at many different wavelengths from 230 nm to 264.3 nm were measured using the method described above. These measurements were carried out with the rotating detector direction perpendicular and parallel to the photolysis laser polarization. TOF spectra at four specific wavelengths are shown in Fig.1. Since the photolysis laser was generated using a frequency doubling scheme, the photolysis laser polarization was fixed to parallel to the molecular beam direction for convenience in this wavelength region. The TOF spectra shown in Fig.1 were then converted to the total product translational energy (E_{trans}) distributions.

Since the total product translational energy (E_{trans}) deposited into the two products (H and N_3) can be written as [16,26]

$$E_{\text{trans}} = h\nu + E_{\text{int}}(HN_3) - D_0(H-N_3) - E_{\text{int}}(N_3) \quad (3)$$

where $h\nu$ is the photon energy of the photolysis laser,

DOI:10.1088/1674-0068/20/04/345-351

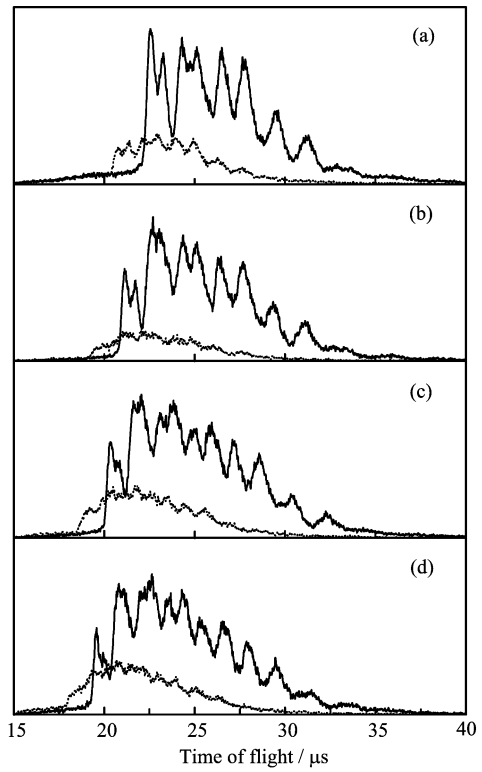

FIG. 1 TOF spectrum recorded at the photolysis wavelengths of (a) λ=248 nm, (b) λ=240 nm, (c) λ=235 nm, (d) λ=230 nm, with the MCP detector perpendicular to the laser polarization (solid lines) and parallel to the laser polarization (dotted lines).

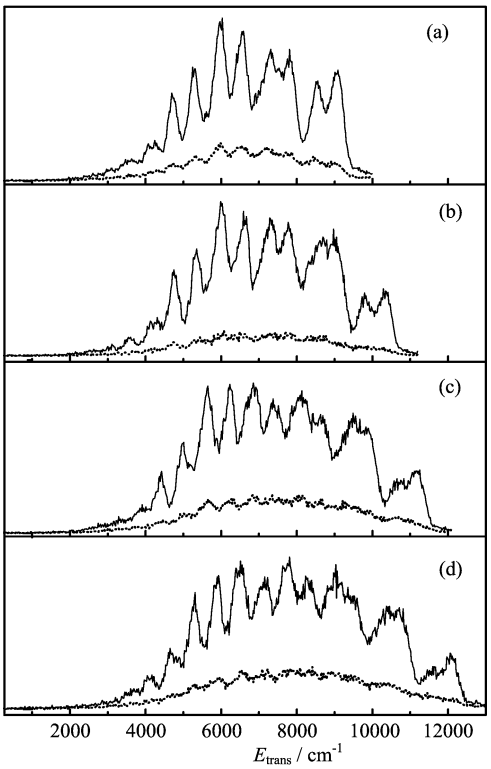

FIG. 2 The product transitional energy ($E_{\rm trans}$) distribution derived from the experimentally measured H atom TOF spectra recorded at (a) λ=248 nm, (b) λ=240 nm, (c) λ=235 nm, (d) λ=230 nm, with θ=90° (dotted lines), 0° (solid lines).

$E_{\rm int}(HN_3)$ is the internal energy of the HN_3 molecule, $D_0(H-N_3)$ is the dissociation energy of the $H-N_3$ bond and $E_{\rm int}(N_3)$ is the internal energy of the N_3 product. HN_3 is cooled down to very low temperature in the supersonic expansion beam, therefore $E_{\rm int}(HN_3)\cong 0$. $E_{\rm trans}$ can then be simplified to:

$$E_{\rm trans} = h\nu - D_0(H-N_3) - E_{\rm int}(N_3) \qquad (4)$$

The total product translational energy distribution is also the internal energy distribution of the N_3 product. Thus, the structures observed in the product translational energy distribution are all due to the ro-vibrationally excited N_3 products. Here the photolysis energy, $h\nu$, is known exactly. From Eq.(4), if the maximum translational energy limit ($E_{\rm TMAX}$) in the product translational energy distribution corresponds to the N_3 ground ro-vibrational state, $D_0(H-N_3)$ should be equal to $h\nu - E_{\rm TMAX}$. Using the extrapolated onset of $E_{\rm TMAX}$ in Fig.2, the $H-N_3$ bond energy, $D_0(H-N_3)$ is determined to be 30910±100 cm^{-1}. This result is consistent with the value obtained by Cook *et al.*, $D_0(H-N_3)$=30970±50 cm^{-1} [15] and with the value by Zhang *et al.*, $D_0(H-N_3)$=31020±180 cm^{-1} [16].

The vibrational structures observed in all the translational energy distribution at all photolysis wavelengths studied here show a clear progression of doublets. These structures, given the availability of accurate theoretical vibrational term values [21], could be assigned to a progression in the N_3 symmetric stretching mode (characteristic spacing ∼1320 cm^{-1}), (v_1,0,0), together with a progression of the symmetric stretching mode with one quantum of bending motion, (v_1,1,0), as did in previous similar works by Cook *et al.* [15] and Zhang *et al.* [16].

In order to understand how the nascent N_3 product vibrational state distribution changes with the photolysis energy, we have also carried out a wavelength dependence study of the HN_3 photodissociation. Figure 3 shows an experimental translational energy spectrum obtained at 235 nm. In the simulation, a full width half maximum (FWHM) of 400 cm^{-1} is used. In one of the simulation, we have included (lower panel in Fig.3) only progressions of the (v_1,0,0) and (v_1,1,0) vibrational series assuming only v_2=0,1 vibrational states are excited. Clearly, it is hard to simulate satisfactorily the translational energy spectrum. However, by including the series of (v_1,2,0), the fitting to the translational energy spectrum is much improved (middle panel in Fig.3). This suggests that the N_3 products with v_2=2 (v_1,2,0) vibrationally excitation are also likely present. By including the three series of the vibrational states, we have successfully simulated all the translational en-

DOI:10.1088/1674-0068/20/04/345-351

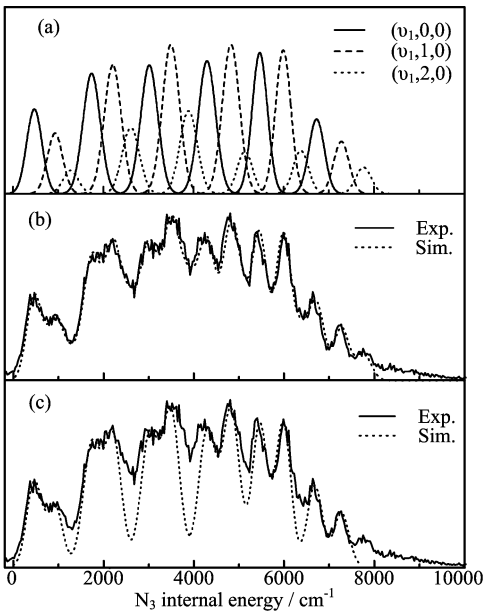

FIG. 3 Experimentally derived internal energy profiles together with simulations for photolysis of HN_3 at λ=235 nm. (a) Individual contributions of N_3 vibratioal state products; (b) includes progressions in the (v_1,0,0), (v_1,1,0) and (v_1,2,0) modes; (c) only progressions in the (v_1,0,0) and (v_1,1,0) modes are included.

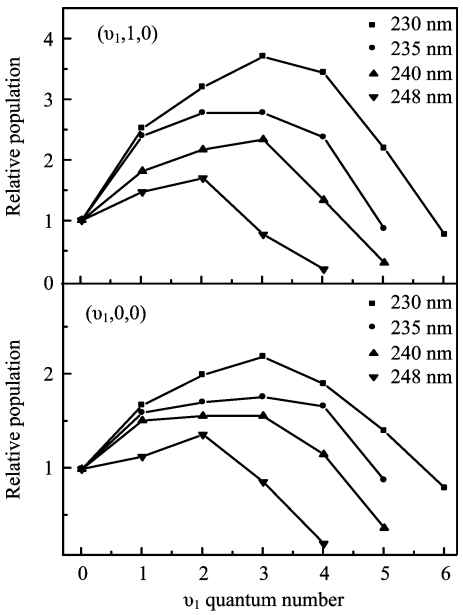

FIG. 4 Relative populations of all clearly resolved $N_3(X)$ vibrational states at four different photolysis wavelengths were obtained for both (v_1,0,0) and (v_1,1,0) series. Here, we normalized the population of the first vibrational state to 1.

ergy spectra at the photolysis wavelengths from 225 nm to 254 nm. In the translational energy spectrum shown in Fig.3, most of the N_3 vibrational structures are not well resolved. However, the peak at $\sim$7900 cm^{-1} in the translational energy distribution at the photolysis wavelength of 235 nm shown in Fig.3, which can be clearly assigned to the (5,2,0) vibrational state, strongly supports the argument that the (v_1,2,0) vibrationally excited N_3 products are present.

From the translational energy distributions shown in Fig.2, the average transition energy ($\langle E_{\rm trans}\rangle$) at 230, 235, 240, and 248 nm are determined to be 64.6%, 66.5%, 68%, and 73%, respectively. The translational energy percentage decreases as photolysis energy decreases. The relative populations of (v_1,0,0) and (v_1,1,0) ($v_1\leq$6) different vibration states were also determined and shown in Fig.4. In this figure, the relative population of the lowest vibrational state at each photolysis wavelength is normalized to one. Clearly, the vibrational excitation of the v_1 mode increases as the photolysis energy increases. As photolysis energy increases, the v_2=1 state population also increases relative the v_2=1 state. This indicates the vibrational excitation of the N_3 radical increases in both vibrational modes that are excited. It is interesting to point out, however, that the rotational excitation of the N_3 product remains almost the same since the peak width in the translational energy distributions are similar in this photolysis energy regime.

Since product translational energy distributions, or N_3 product internal energy distribution can be obtained, were determined at two different detection directions that are perpendicular or parallel to the photolysis laser polarizations in this experiment, product angular anisotropy parameters can also be derived.

Figure 5(a) shows the translational energy dependent product anisotropy parameter obtained for the photolysis energy of 240 nm. Between the translational energy range of 2000-11000 cm^{-1}, the anisotropy parameter is between -0.7 to -0.8, and is only weakly dependent on the translational energy. It is noted that anisotropy parameters below the translational energy of 2000 cm^{-1} is not provided because no signal is observed in this range at the photolysis wavelengths described here. Anisotropy parameter at other photolysis wavelengths in this photolysis energy region shows similar behaviors. The overall anisotropy parameter at different photolysis wavelengths in this regime only varies slightly.

Figure 6 shows the overall angular anisotropy parameters at the photolysis wavelengths of 264.3 nm to 188 nm, in which the overall anisotropy parameters at the photolysis wavelengths from 264.3 nm to 230 nm are all around -0.7. These results suggest that the photodissociation dynamics of HN_3 in this photolysis energy regime is similar, and the dissociation occurs directly via the excited potential energy surface to produce a linear N_3 radical product. This conclusion is quite consistent with previous experimental results by Cook *et al.* [15] and Zhang *et al.* [16].

DOI:10.1088/1674-0068/20/04/345-351

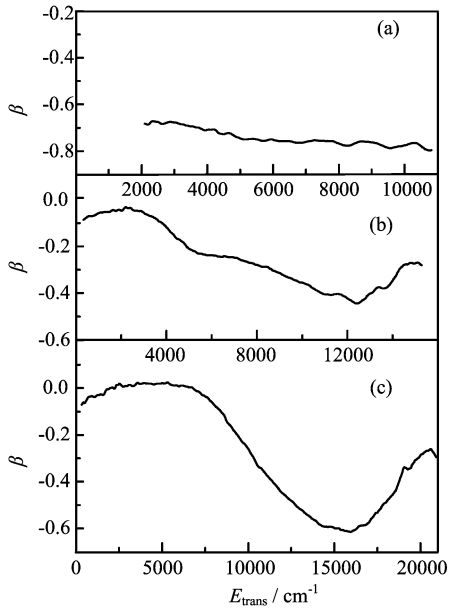

FIG. 5 Anisotropy parameter β as a function of the total transitional energy (E_{trans}) at three typical photolysis wavelengths: (a) λ=240 nm, (b) λ=217 nm, and (c) λ=193.3 nm.

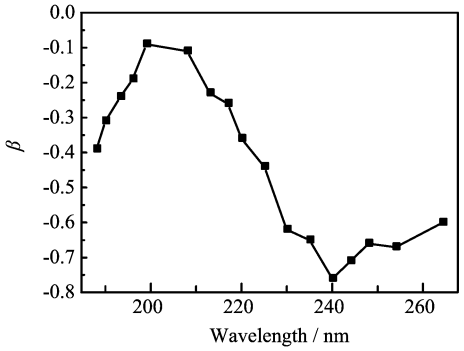

FIG. 6 The photolysis wavelength dependence of the overall angular anisotropy parameter β.

B. Dynamics from 225 nm to 213 nm

Figure 7 shows that the TOF spectra of the H-atom product obtained at the photolysis wavelengths of 225, 220, 217, and 213 nm with the detector at both the perpendicular and parallel directions. Since photolysis laser wavelengths below 225 nm was generated using a frequency mixing scheme as described above, the photolysis laser polarization was fixed to be perpendicular to the molecular beam direction for convenience in this wavelength region. The TOF spectra were converted to the product translational energy distributions, and are shown in Fig.8. From this figure, the dynamical feature in the translational energy distribution starts to become a little congested and the vibrational structures eventually disappear all together at the 213 nm photodissociation. This is likely due to the larger rotational

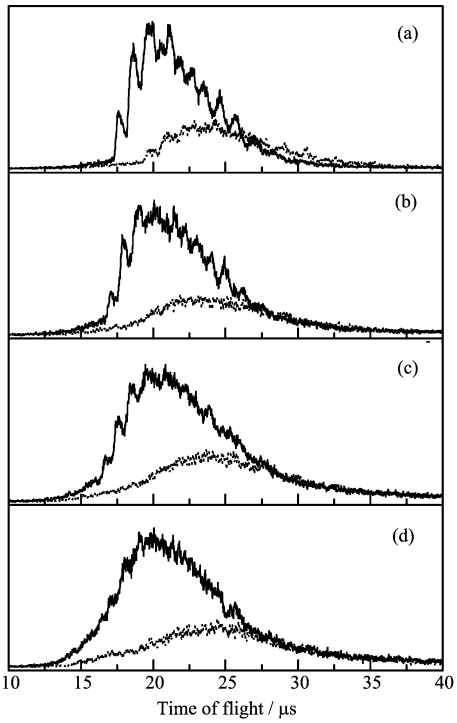

FIG. 7 TOF spectrum recorded at the photolysis wavelengths of (a) λ=225 nm, (b) λ=220 nm, (c) λ=217 nm, and (d) λ=213 nm, with the MCP detector perpendicular to the laser polarization (solid lines) and parallel to the laser polarization (dotted lines).

excitation of the N_3 product because more available energy is deposited into the internal degrees of freedom of the N_3 radical product. Furthermore, as the photolysis energy increases, the overall product angular anisotropy parameter decreases noticeably. From Fig.6, the overall anisotropy parameter decreases from -0.6 to -0.1 in this wavelength regime, suggesting the dynamics is significantly altered in this range. From the translational energy distributions shown in Fig.7, this change of the angular anisotropy can be traced to two dynamical origins: the decrease of the overall anisotropy of the main dynamical feature and the appearance of an isotropic slow component.

The most interesting change of the dynamics in this wavelength range is the appearance of a slow peak starting from 225 nm. As the photolysis energy increases, this peak seems to become more important. From the translational energy dependent anisotropy parameter at the photolysis wavelength of 213 nm (Fig.5(b)), the anisotropy parameter is almost zero in the low translational energy region. This is obviously due to the fact that the angular distribution of the slow component is isotropic. At higher translational energy, the anisotropy parameter is about -0.4 at this photolysis wavelength, which is also significantly smaller than the value in the low photolysis energy region (230-248 nm). This supports our argument that the overall decrease of

DOI:10.1088/1674-0068/20/04/345-351

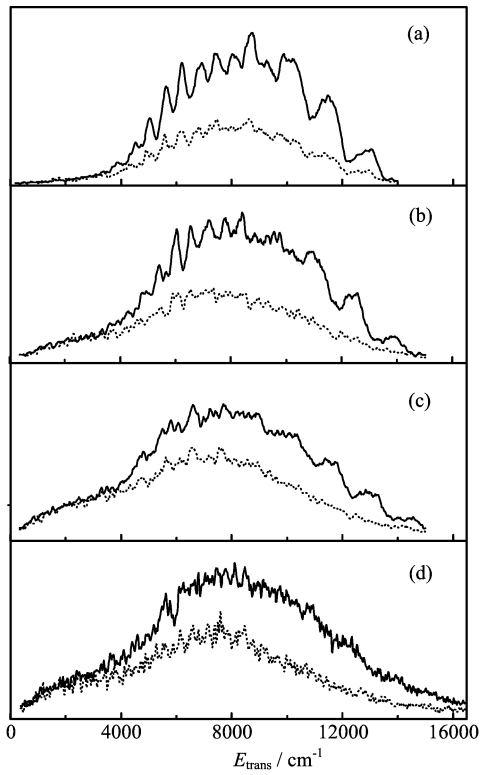

FIG. 8 The product transitional energy ($E_{\rm trans}$) distribution derived from experimentally measured H atom TOF spectra at the photolysis wavelength of (a) λ=225 nm, (b) λ=220 nm, (c) λ=217 nm, and (d) λ=213 nm, with θ=90° (solid lines), 0° (dotted lines).

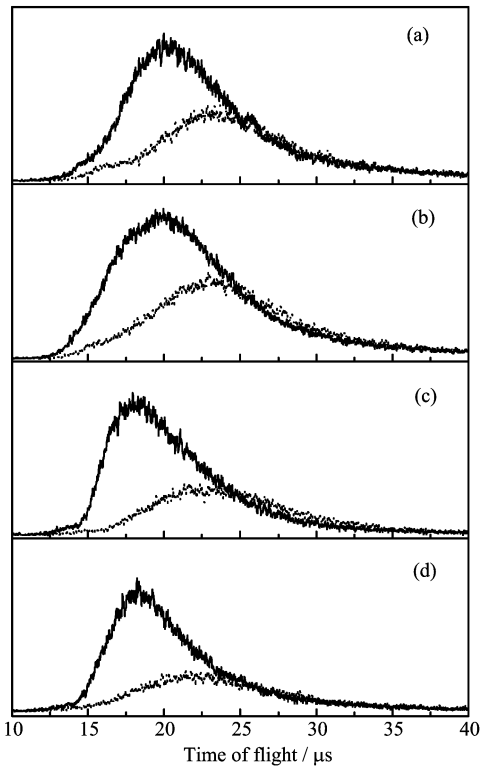

FIG. 9 TOF spectrum recorded at the photolysis wavelengths of (a) λ=208 nm, (b) λ=199 nm, (c) λ=193.3 nm, and (d) λ=190 nm, with the MCP detector perpendicular to the laser polarization (solid lines) and parallel to the laser polarization (dotted lines).

the anisotropy parameter is partly due to the anisotropy decrease of the main dynamics feature at higher translational energies.

The appearance of the slow feature in this wavelength regime turns out to be dynamically quite interesting. Recent theoretical studies show that the energy of appearance is coincident with the threshold of the ring closure pathway of the HN_3 molecule, suggesting that the slow feature corresponds to the cyclic N_3 product [27]. This is also consistent with the fact that the product angular distribution for this feature is isotropic.

C. Photodissociation dynamics from 208 nm to 190 nm

TOF spectra of the H-atom product were also measured at the even shorter photolysis wavelengths. Four TOF spectra at the photolysis wavelengths of 208, 199, 193.2, and 190 nm with the detector at both the perpendicular and parallel directions to the laser polarization are shown in Fig.9. The photolysis laser polarization was also fixed to be perpendicular to the molecular beam direction for convenience in this wavelength region. The product translational energy distributions converted from these TOF are shown in Fig.10. From these translational energy distributions, translational energy product anisotropy parameters can also be determined. From Fig.6, the overall product anisotropy parameter increases starting from 208 nm. Figure 5(c) shows the typical translational energy dependent anisotropy parameters at the photolysis wavelength of 193.3 nm. At the low translational energy region, the anisotropy parameter remains to be zero as in 217 nm photolysis. The increase of the overall anisotropy is due to the increase of the anisotropy of the fast component. In Fig.5(c), the maximum anisotropy parameter at higher translational energies is about −0.6, noticeably larger than that at the 217 nm photolysis. This can be likely due to that fact that different electronic states B and C are becoming accessible at shorter wavelengths.

In comparison with previous photodissociation study at 193.3 nm by Zhang *et al.* [16], noticeable difference was found in both the transitional energy distribution and the energy dependent angular anisotropy between the result of this work and that by Zhang *et al.* During the experiment in this work, we found the HN_3 photodissociation around 193.3 nm can easily be complicated by multiphoton processes. Therefore, we tried to lower the photolysis laser power as much as possible to reduce the multiphoton effect to minimum in the experiment.

DOI:10.1088/1674-0068/20/04/345-351

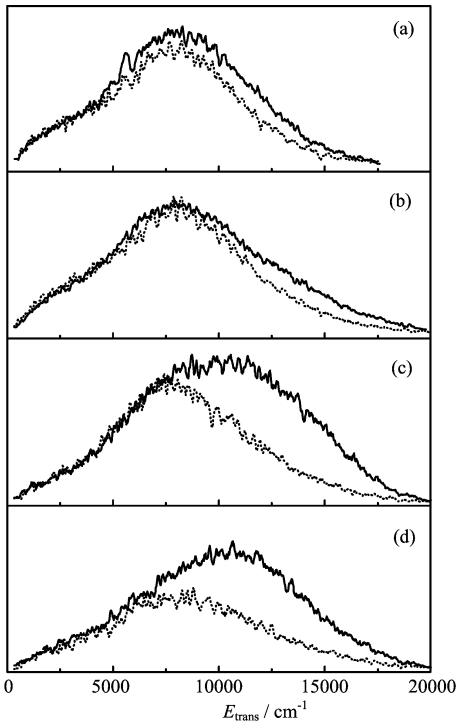

FIG. 10 The product transitional energy ($E_{\rm trans}$) distribution derived from experimentally measured H atom TOF spectra recorded at (a) λ=208 nm, (b) λ=199 nm, (c) λ=193.3 nm, and (d) λ=190 nm, with θ=90° (solid lines), 0° (dotted lines).

IV. CONCLUSION

Ultraviolet photodissociation of HN_3 has been investigated in the photolysis wavelength range of 188 nm to 264.3 nm using the H-atom Rydberg tagging time-of-flight method. Time-of-flight spectra of the H atom product were measured at the detection directions both perpendicular and parallel to the photolysis laser polarization direction. Total product translational energy distributions as well as product angular anisotropy parameters were determined for the H+N_3 channel at total 12 different photolysis wavelengths. The vibrational state distributions of the linear N_3 product has also been derived at the photolysis wavelengths from 230 nm to 254 nm. Above photolysis wavelength 225 nm, HN_3 predominantly dissociate through the repulsive state and the linear N_3 product vibrational state distributions have been determined for this region. Below 225 nm, a new slow channel starts to appear in addition to the existing direct channel. The appearance energy of this channel is coincident with the theoretical energy threshold of the ring closure pathway of the HN_3 molecule, suggesting that a cyclic N_3 formation is likely present. At even higher photolysis energies, the change of dissociation dynamics is clearly noticeable. This is likely due to the fact that the different electronic excited states are excited at higher photolysis energies.

V. ACKNOWLEDGMENTS

This work was supported by Chinese Academy of Sciences via the grant of the CAS international collaboration group, and also partly by the Ministry of Science and Technology of China and the National Natural Science Foundation of China.

[1] H. Okabe, *Photochemistry of Small Molecules*, New York: Wiley, 287 (1978).
[2] J. R. McDonald, J. W. Rabalais, and S. P. McGlynn, J. Chem. Phys. **52**, 1332 (1970).
[3] J. W. Rabalais, J. R. McDonald, V. Scherr, and S. P. McGlynn, Chem. Rev. **71**, 73 (1970).
[4] A. P. Baronavski, R. G. Miller, and J. R. McDonald, Chem. Phys. **30**, 119 (1978).
[5] U. Meier and V. Staemmler, J. Phys. Chem. **95**, 6111 (1991).
[6] J. J. Chu, P. Marcus, and P. J. Dagdigian, J. Chem. Phys. **93**, 257 (1990).
[7] F. Rohrer and F. Stuhl, J. Chem. Phys. **88**, 4788 (1988).
[8] K. H. Gericke, T. Hass, M. Lock, R. Thienl, and F. J. Comes, J. Phys. Chem. **95**, 6104 (1991).
[9] K. H. Gericke, M. Lock, R. Fasold, and F. J. Comes, J. Chem. Phys. **96**, 422 (1992).
[10] H. H. Nelson and J. R. McDonald, J. Chem. Phys. **93**, 8777 (1990).
[11] M. Hawley, A. P. Baronavski, and H. H. Nelson, J. Chem. Phys. **99**, 2638 (1993).
[12] K. H. Gericke, M. Lock, and F. J. Comes, Chem. Phys. Lett. **186**, 427 (1991).
[13] M. Lock, K. H. Gericke, and F. J. Comes, Chem. Phys. **213**, 385 (1996).
[14] T. Haas, K. Gericke, C. Maul, and F. J. Comes, Chem. Phys. Lett. **202**, 108 (1993).
[15] P. A. Cook, S. R. Langford, and M. N. R. Ashfold, Phys. Chem. Chem. Phys. **1**, 45 (1999)
[16] J. Zhang, K. Xu, and G. Amaral, Chem. Phys. Lett. **299**, 285 (1999).
[17] A. E. Douglas and W. J. Jones, Can. J. Phys. **43**, 2216(1965).
[18] R. A. Beaman, T. Nelson, D. S. Richards, and D. W. Setser, J. Phys. Chem. **91**, 6090 (1987).
[19] C. R. Brazier, P. F. Bernath, J. B. Burkholder, and C. J. Howard, J. Chem. Phys. **89**, 1762 (1988).
[20] R. Pahnke, S. H. Ashworth, and J. M. Brown, Chem. Phys. Lett. **147**, 179 (1988).
[21] G. Chambaud and P. Rosmus, J. Chem. Phys. **96**, 77 (1991).
[22] L. Schnieder, K. Seekamp-Rahn, E. Wrede, and K. H. Welge, J. Chem. Phys. **107**, 6175 (1997).
[23] L. Schneider, W. Meier, K. H. Welge, M. N. R. Ashfold, and C. Western, J. Chem. Phys. **92**, 7027 (1990).
[24] M. Qiu, Z. Ren, L. Che, D. Dai, S. Harich, X. Wang, and X. Yang, Chin. J. Chem. Phys. **19**, 93 (2006).
[25] B. Krakow, R. C. Lord, and G. O. Neely, J. Mol. Spectrosc. **27**, 148 (1968).
[26] J. Zhang, M. Dulligan, and C. Wittig, J. Phys. Chem. **99**, 7446 (1995).
[27] J. Zhang, P. Zhang, Y. Chen, K. Yuan, S. A. Harich, X. Wang, Z. Wang, X. Yang, K. Morokuma, and A. M. Wodtke, Phys. Chem. Chem. Phys. **8**, 1690 (2006).

DOI:10.1088/1674-0068/20/04/345-351